ACTUATORS

# Biohybrid robot powered by an antagonistic pair of skeletal muscle tissues

Yuya Morimoto,[1] Hiroaki Onoe,[1,2] Shoji Takeuchi[1,3]*



**Biohybrid robots are attracting attention as promising candidates to enhance robot applicability to studies on biological designs and in vitro construction of biological dynamic systems. Rapid progress in biohybrid robots with skeletal muscle tissues formed on a flexible substrate has enabled various types of locomotion powered by muscle tissue. However, it has been difficult to achieve high levels of both large and long-term actuations of the skeletal muscle tissues because of their spontaneous shrinkage through the course of the tissue culture. To overcome this limitation, we adapted the concept of biological systems and developed a biohybrid robot actuated by an antagonistic pair of skeletal muscle tissues. Our robot achieved large actuation (~90° of rotation of a joint) by selective contractions of the skeletal muscle tissues and a long lifetime (~1 week) by balancing tensions of the antagonistic tissues to prevent the spontaneous shrinkage. As a demonstration, we showed that our biohybrid robots allowed a pick-and-place manipulation of objects. This research may provide a platform to exceed the limitations of design in conventional biohybrid robots and replicate various lifelike movements.**

## INTRODUCTION

Recent advances in biofabrication techniques have achieved integration of engineered muscle tissues with artificial devices, leading to biohybrid robots that allow us to understand the design strategy of living organisms and to engineer their dynamic systems (*1*). Conventionally, many researchers have proposed biohybrid robots composed of a muscle tissue cultured on a flexible substrate and have succeeded in deformation of the substrate by contractions of the muscle tissues (*2*, *3*). These robots enabled biomimetic movements—such as pumping (*4*), grasping (*5*–*7*), walking (*7*–*10*), and swimming (*11*–*14*)—by using design strategies based on the hearts, claws, inchworms, and aquatic organisms, respectively. Mainly cardiac and skeletal muscle tissues have been used as the muscle tissues for biohybrid robots because their contractions are generated by applying external stimulation, such as electrical (*5*–*7*, *9*, *11*) and optical (*10*, *13*) stimulations. In particular, skeletal muscle tissues are attractive driving elements owing to precise controllability of their contractions, in contrast to cardiac muscle tissues. However, the contractions of the skeletal muscle tissues on flexible substrates do not last for a long time due to spontaneous shrinkage of the tissues caused by their intrinsic traction force that increases through the course of culture (*9*, *15*). This spontaneous shrinkage makes the skeletal muscle tissues much shorter than their initial length, leading to contraction malfunction. Although culturing the tissues on a rigid substrate may prevent spontaneous shrinkage (*16*–*23*), the tissue contraction is isometric because of the high stiffness of the substrate. Thus, such a configuration is not suitable as a biohybrid actuator. Consequently, it is difficult to achieve compatibility between large actuation and a long lifetime in a biohybrid robot. On the other hand, biological systems overcome these issues by using antagonistic pairs of skeletal muscles. The selective contractions of each skeletal muscle allow large actuation, and balancing the tension using antagonistic muscles prevents their spontaneous shrinkage over the long term.

In this study, we developed a biohybrid robot actuated by an antagonistic pair of skeletal muscle tissues (Fig. 1A). To take the advantage of the antagonistic pair of skeletal muscle tissues, the biohybrid robot has a joint connected to the skeletal muscle tissues via flexible ribbons. Contractions of each skeletal muscle tissue are controlled by applying electrical stimulations with gold electrodes. When the skeletal muscle tissues contract selectively, linear contraction and extension of the skeletal muscle tissues can induce a smooth bidirectional rotation of the joint, leading to large actuation of the biohybrid robot. Furthermore, because the tensions of both skeletal muscle tissues changed similarly during culture, their contractility was maintained for a long time (~1 week) without notable spontaneous shrinkage. We investigated the contractile properties of the skeletal muscle tissues and analyzed the actuations of the biohybrid robot. As examples of usage, we demonstrate that the biohybrid robots can manipulate an object by controlling their actuations through contractions of the skeletal muscle tissues.

## RESULTS

### Construction of a biohybrid robot powered by an antagonistic pair of skeletal muscle tissues

The fabrication process for the biohybrid robot with an antagonistic pair of skeletal muscle tissues has two steps. The first step is the preparation of a robot skeleton. The skeleton consists of a joint, pairs of electrodes, anchors for skeletal muscle tissues, and flexible ribbons bridged between the anchors and the joint (fig. S1A). The body of the skeleton and the anchors were fabricated by stereolithography, and the electrodes were produced by parylene-based standard photolithography (fig. S1B, i to v). The joint in the skeleton can be rotated when the flexible ribbon is pulled (Fig. 1A). This mechanism mimics the musculoskeletal system of the living body; the joint driving mechanism observed in the musculoskeletal system enables efficient force transmission of skeletal muscles (*24*). In addition, parylene-coated gold electrodes placed near the anchors

[1]Center for International Research on Integrative Biomedical Systems, Institute of Industrial Science, University of Tokyo, Tokyo 153-8505, Japan. [2]Department of Mechanical Engineering, Keio University, Yokohama, Kanagawa 223-8522, Japan. [3]International Research Center for Neurointelligence, University of Tokyo Institutes for Advanced Study, University of Tokyo, Tokyo 153-8505, Japan.
*Corresponding author. Email: takeuchi@iis.u-tokyo.ac.jp

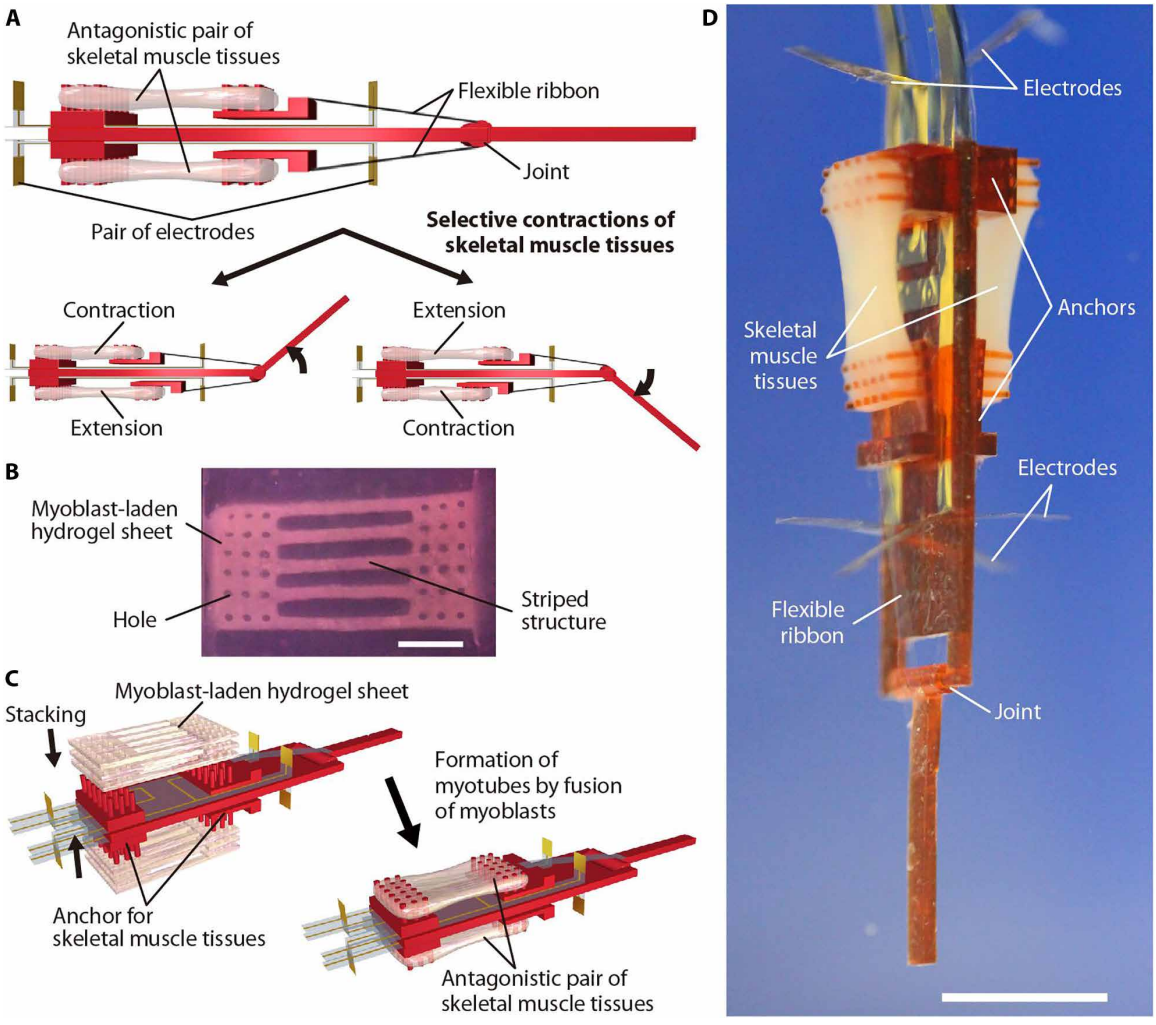


**Fig. 1. Construction of a biohybrid robot with an antagonistic pair of skeletal muscle tissues.** (**A**) Illustrations of a biohybrid robot with an antagonistic pair of skeletal muscle tissues and bidirectional motion of the biohybrid robot by selective contractions of the skeletal muscle tissues. (**B**) An image of a myoblast-laden hydrogel sheet shaped with a PDMS stamp. (**C**) Construction of an antagonistic pair of skeletal muscle tissues by stacking and culturing the myoblast-laden hydrogel sheets on the skeleton in symmetrical positions. (**D**) Image of the biohybrid robot with the antagonistic pair of skeletal muscle tissues. Scale bars, 2 mm (B) and 5 mm (D).

allow application of electrical stimulations to an antagonistic pair of skeletal muscle tissues individually.

The second step is the formation of skeletal muscle tissues on the skeleton (Fig. 1C). We first prepared myoblast-laden hydrogel sheets using polydimethylsiloxane (PDMS) stamps (Fig. 1B, and fig. S2, A and B) and then stacked the sheets onto the immobilized anchors to form three-dimensional (3D) tissues with large cross-sectional areas (figs. S1B, vi to viii, and S2C). The sheets had holes at their edges and striped structures. The holes were used to place the sheets through the pillars on the anchors. The striped structures were designed to promote alignment of myoblasts, as cells in a striped structure are known to align along its long axis (*17*, *25*). After 2 days of culture of the myoblast-laden hydrogel sheets, we found that the sheets became handleable in culture medium by the combination of the increased cell-cell contact and increased compaction of the hydrogel. When we stacked the myoblast-laden hydrogel sheets onto the anchors of the skeleton (fig. S3A), we confirmed that the edges of the sheets were fixed to the pillars on the anchors via the holes, showing that our method allows culture of myoblasts with maintenance of their lengths, as do conventional methods (*18*–*23*). We also confirmed that gaps between the striped structures were maintained after the stacking, which promoted the diffusion of culture medium and oxygen into the stacked sheets. As the culture proceeded, the striped structures were fused into a single construct, resulting in the formation of an antagonistic pair of skeletal muscle tissues on the skeleton (fig. S3A). Optical coherence tomography (OCT) imaging of the skeletal muscle tissue revealed that all 14 of the striped structures were integrated at the center and that the tissue had a large cross-sectional area ($2.5 \pm 0.3$ mm$^2$, $n = 5$ tissues at the center; means ± SD) achieved by integration of the structures (cross-sectional area, ~0.25 mm$^2$) (fig. S3B). After the release of the formerly immobilized anchors (fig. S1B, vii and viii), we confirmed that the tensions of both skeletal muscle tissues were balanced through the joint in the biohybrid robot (Fig. 1D and fig. S4). In this state, the skeletal muscle tissues tended to have different lengths ($4.1 \pm 0.3$ mm, $n = 14$ skeletal muscle tissues in seven biohybrid robots; means ± SD) compared to their cultured length (4 mm). We think that the differences in their length were caused by an

imbalance of tensions at their cultured length and errors in the skeleton from fabrication with manually assembled parts, such as deviation of the anchor position and differences in the flexible ribbon lengths.

To demonstrate the advantages of the striped structures in the myoblast-laden hydrogel sheets, we investigated the relationship between the dimensions of the myoblast-laden hydrogel structures and the contractile force of the skeletal muscle tissue fabricated by culturing in the structures (fig. S5). The result showed that narrower striped structures allow an increase in the contractile force per cross-sectional area. This increase in the contractile force was probably owing to the facilitation of myotube orientation because myotube orientation is increased when cells are cultured in the narrow striped structure (*17*). Because the skeletal muscle tissues on the biohybrid robot were fabricated by integration of the striped structures, we believe that the skeletal muscle tissues have the potential to generate a high contractile force per unit of cross-sectional area.

### Characteristics of skeletal muscle tissues fabricated by assembling myoblast-laden hydrogel sheets

To characterize the constructed skeletal muscle tissues, we conducted morphological and functional analyses. For the morphological analysis of the skeletal muscle tissues in the biohybrid robot, we prepared axial sectional images of the tissues stained with hematoxylin and eosin (H&E) (Fig. 2A). In the sectional images, cell enucleation was not observed, indicating that our tissue formation method allows maintenance of cell viability during culture without central necrosis in the skeletal muscle tissues. Moreover, the α-actinin, myosin heavy chains, and myogenin arrangements in the skeletal muscle tissues were determined by using a fluorescent immunostaining method. The results of myogenin immunostaining showed that almost all cell nuclei were myogenin-positive [myogenin is a regulatory transcription factor involved in myogenesis (*18*)] (fig. S6), suggesting that myotube formation had proceeded by fusion of myoblasts in the skeletal muscle tissues. Furthermore, we confirmed formation of striped patterns of α-actinin and myosin heavy chains in the myotubes (Fig. 2B), indicating that sarcomeres were formed in the skeletal muscle tissues. The results demonstrate that the engineered skeletal muscle tissues on our biohybrid robot have the fundamental morphology required for contractible striated skeletal muscles and were comparable to skeletal muscle tissues 3D-engineered in culture dishes (*19*–*21*). In addition, the immunostained images and long-axial sectional image show one-directional alignment of the myotubes in the skeletal muscle tissues (Fig. 2, A and B). These morphological analyses suggest that the skeletal muscle tissues constructed using our method were striated skeletal muscle tissues, which enable one-directional contractions, and had the proper morphology of skeletal muscle tissues.

To investigate the function of the skeletal muscle tissues formed by assembling the myoblast-laden hydrogel sheets, we placed the skeletal muscle tissues on a substrate with a cantilever and measured their contractile force according to deformation of the cantilever (*17*, *25*). By applying electrical pulses to the skeletal muscle tissues, we controlled their contractions according to the frequency and magnitude of the electrical field; the duration of the pulse was 2 ms. With electrical pulses at 1 Hz, the contractions were twitches and were synchronized with the electrical pulses. At higher frequencies (over 6.25 Hz), the contractile mode changed from twitch to tetanus by superimposing the twitches (Fig. 2C). As a result, the contractile force increased depending on the frequency of the electrical pulses. The peak-to-peak (p-p) contractile forces of twitch and tetanus also increased with respect to the magnitude of the electrical field, becoming saturated to almost constant value at over 1 V/mm (Fig. 2D). These changes in their contractile force relative to electrical pulses show the same tendency as that seen in conventionally engineered skeletal muscle tissues (*22*, *23*). From these functional analyses, we confirmed that the constructed tissues had the contractility unique to skeletal muscle tissues. Moreover, to investigate the appropriate number of culture days needed to maximize the contractile force, we measured the p-p contractile force from culturing for different numbers of days (Fig. 2E). During the culture, the contractile force peaked on day 10. We think that the proliferation of fibroblasts might cause the decrease in the p-p contractile force after day 15 because fibroblasts are normally contained in myoblasts isolated from neonatal rats (*19*). Therefore, we decided to use 10 days as the culture time for skeletal muscle tissues in the following experiments.

To evaluate the effects of the striped structures in the myoblast-laden hydrogel sheets, we compared the contractile force of skeletal muscle tissues fabricated using myoblast-laden hydrogel sheets with striped structures and those of skeletal muscle tissues fabricated using myoblast-laden hydrogel blocks without the striped structures (fig. S7). Both the twitch and tetanus of the skeletal muscle tissues fabricated from multiple striped structures exhibited a stronger force than did those of the tissue fabricated from the hydrogel block without the striped structures (Fig. 2F). Therefore, the comparison of the contractile force shows that assembling the tissue from myoblast-laden hydrogel sheets with striped structures is an appropriate method to form skeletal muscle tissues with high contractile force.

Furthermore, we investigated the length-force relationship of the skeletal muscle tissues. In the relationship between length and contractile force, their contractile force had a vertex around the center of the length-force curve when we changed their length by about ±25% from their culture length (Fig. 2G). In the relationship between length and passive force (shrinking force caused by the intrinsic elastic properties of skeletal muscle tissues), their passive force increased in an accelerated manner with stretching of the skeletal muscle tissues (Fig. 2H). These results indicate that the length-force relationship of the skeletal muscle tissues corresponded to the characteristics of in vivo skeletal muscle (*26*). In addition, the result of the length–passive force relationship indicates that the skeletal muscle tissues were cultured under passive force, with their length longer than their natural length; the passive force is important for formation of aligned myotubes in skeletal muscle tissues (*15*). Although increasing the passive force through elongation of a skeletal muscle tissue works as an anti-force to oppose the contractions of an antagonistic skeletal muscle tissue in our biohybrid robot, we consider that the skeletal muscle tissues fabricated with our method are appropriate driving elements for the biohybrid robot because the contractile force is much stronger than the passive force.

### Actuation of biohybrid robots with contractions of skeletal muscle tissues

We confirmed the actuation of biohybrid robots by controlling the contractions of the skeletal muscle tissues. The contractions of one skeletal muscle tissue were induced by electrical fields generated

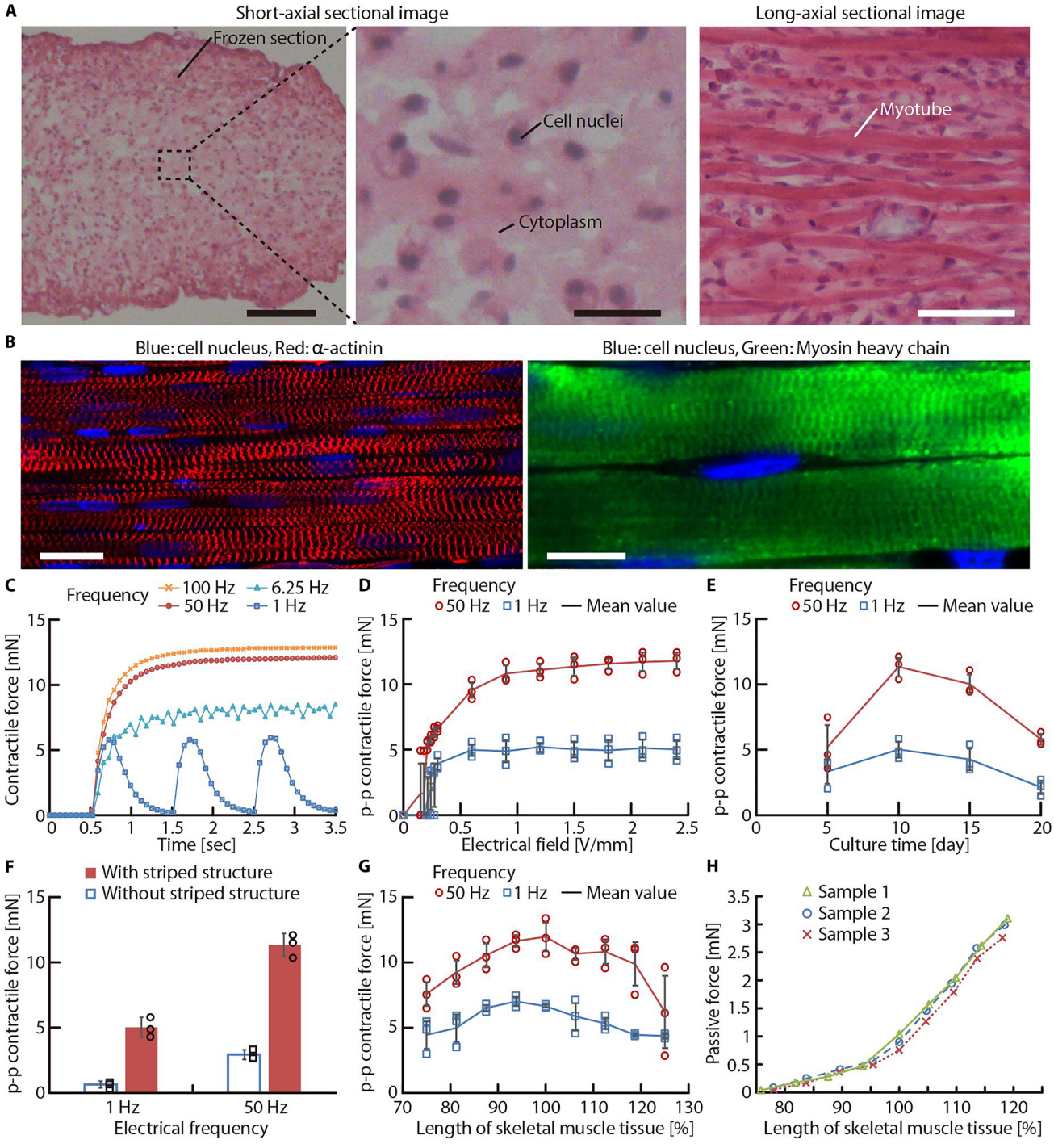


**Fig. 2. Properties of skeletal muscle tissues fabricated with myoblast-laden hydrogel sheets.** (**A**) Short-axial sectional images (left and middle) and long-axial sectional images (right) of skeletal muscle tissues stained with H&E in our biohybrid robot. (**B**) Confocal images of the skeletal muscle tissues in the biohybrid robot with the following tissue immunostaining: cell nucleus (blue), α-actinin (red), and myosin heavy chain (green). (**C**) Temporal variation of contractile force of skeletal muscle tissues depending on the different electrical frequencies applied (electrical field, 1.5 V/mm; duration, 2 ms). (**D**) The p-p contractile force of different skeletal muscle tissues ($n$ = 3) after changes in the applied electrical field (duration, 2 ms). (**E**) Changes in the p-p contractile force of different skeletal muscle tissues ($n$ = 3) during culture (electrical field, 1.5 V/mm; duration, 2 ms). (**F**) Changes in the p-p contractile force of different skeletal muscle tissues fabricated using myoblast-laden hydrogel sheets with striped structures ($n$ = 3) and those fabricated using myoblast-laden hydrogel blocks without the striped structures ($n$ = 3) (electrical field, 1.5 V/mm; duration, 2 ms) (means ± SD). (**G**) Plots of the p-p contractile force of different skeletal muscle tissues ($n$ = 3) relative to their length (the reference length is their culture length; electrical field, 1.5 V/mm; duration, 2 ms). (**H**) Plots of the passive force of different skeletal muscle tissues ($n$ = 3) depending on their length. (A to D and F to H) Skeletal muscle tissues were cultured for 10 days after stacking the myoblast-laden hydrogel sheets. All error bars show SD. Scale bars, (A) 100 μm (left), 20 μm (middle), 50 μm (right); (B) 20 μm (left), 10 μm (right).

between a pair of electrodes located at both edges of the tissue. Note that muscle contractions were not induced when we applied electrical pulses via the other pair of electrodes located on the opposite side (fig. S8). The biohybrid robot achieved bidirectional rotation of the joint (Fig. 3A and movie S1) when we sequentially applied electrical pulses (electrical field, 1.5 V/mm; frequency, 50 Hz; duration, 2 ms) to each skeletal muscle tissue. By tracking its motions, we measured the rotation angle θ, as shown in Fig. 3A, and the strain of the skeletal muscle tissues relative to their culture length; the strain is expressed as $(L - L_0)/L_0$, where $L$ is the length of the skeletal muscle tissue and $L_0$ is the culture length (Fig. 3, B and C). The profile of the rotation angle was consistent with the profile of strain, showing that contractions of the skeletal muscle tissues caused the rotation of the joint. Moreover, the profile of strain also shows that the skeletal muscle tissues achieved antagonistic movements. Although the skeletal muscle tissues showed different strains in the absence of electrical stimulation, the ranges of both strains during the actuation were almost the same (~0.27). These results indicate that the linear actuation of the skeletal muscle tissues was transferred to the bidirectional rotation of the joint as expected in the design of the skeleton, resulting in an amplification of motions similar to that of the musculoskeletal system of the body. To examine the magnitude of the bidirectional rotation produced according to the properties of applied electrical pulses, we selectively applied electrical pulses with different frequencies and magnitudes of the electrical field to the skeletal muscle tissues (movie S2). In this test, we measured the range of the rotation angle of the joint and the strain of the skeletal muscle tissues during a single cycle of the bidirectional rotation (Fig. 3, D and E). The results show that the magnitudes of the actuations were controllable depending on the frequency and magnitude of the electrical field in the electrical pulses. When we selectively applied 1.5 V/mm, 50-Hz electrical pulses to the skeletal muscle tissues, the biohybrid robots achieved the largest actuation, with a 0.2 strain of the skeletal muscle tissues and a 90° joint rotation, indicating that the biohybrid robot had similar motions to that achieved by the living skeletal muscle [0.2 to 0.4 strain (*27*)] and joint movements of a human finger [85° to 100° (*28*)]. In addition, an analysis of the balance of forces in the bidirectional rotation, as shown in section S1, indicated that the friction force at the joint was too large to ignore and that the balance of tensions of the skeletal muscle tissues relative to the friction force at the joint determined the magnitude of the joint rotation.

Furthermore, to examine the lifetime of the biohybrid robot actuation, we compared the temporal changes in the contractile length of three types of skeletal muscle tissues: skeletal muscle tissue in the biohybrid robot, skeletal muscle tissue on a flexible substrate, and free-standing skeletal muscle tissue (Fig. 3F and fig. S9). The contractile length of the free-standing single skeletal muscle tissue markedly decreased by half in a day and to almost 0 after 1 day due to its spontaneous shrinkage. Similarly, the contractile length of the skeletal muscle tissue on a flexible substrate (conventional biohybrid robot) also decreased after a few days due to its spontaneous shrinkage. By contrast, the skeletal muscle tissue in our biohybrid robot did not decrease in contractility, even after a week, resulting in maintenance of the rotation angle of the joint for a week (fig. S9I). In addition, during the week of testing, major spontaneous shrinkage of the muscle tissues did not occur (fig. S9F). These results indicate that the antagonistic pair of skeletal muscle tissues is a suitable configuration to exert long-term actuations in biohybrid robots by maintenance of their length and contractility.

As a demonstration, we let the biohybrid robot pick up and place a ring by selectively applying 50-Hz electrical pulses (1.5 V/mm) to the skeletal muscle tissues (Fig. 4A and movie S3). In the operation, we first induced a contraction of the skeletal muscle tissue not facing the ring to bring the rotation angle θ close to 0 because the rotation angle is not always 0 at the initial state. After approaching the ring in this state, the biohybrid robot hooked it by rotating the joint through a contraction of the skeletal muscle tissue facing it. Subsequently, the ring was carried by a continuous contraction (~40 s) of the skeletal muscle tissue and placed on a pillar in a given position by a contraction of the opposing skeletal muscle tissue. The result shows that the biohybrid robot can manipulate the ring through a finger-like motion owing to selective contraction of antagonistic skeletal muscle tissues. Moreover, we demonstrated the action using two biohybrid robots simultaneously (Fig. 4B and movie S4). After arranging them to face each other across a square frame, we induced a contraction of each skeletal muscle tissue close to the frame to pick up the square frame after the approach process using contractions of the other skeletal muscle tissue. The results of this operation indicate that our biohybrid robots have the potential to reproduce various lifelike movements.

## DISCUSSION

The present work demonstrates that our configuration of an antagonistic pair of skeletal muscle tissues in a biohybrid robot with a joint contributed to large actuation (a rotation angle of the joint close to 90°) and long-term actuation (~1 week) in the robots by selective contractions and maintenance of the muscle tissue length, respectively. Owing to the large actuation, the biohybrid robots performed pick-and-place manipulations of an object. This demonstration indicates that the biohybrid robots would exceed the limitations of design in conventional biohybrid robots that have been restricted to actuate like a mollusk.

Although a biohybrid robot powered by two explanted frog semitendinosus muscles had been proposed previously as a biohybrid robot with a joint driven by muscle contractions (*29*), usage of explanted muscle caused restriction of the robot dimensions and configuration and a short lifetime (~42 hours) of its actuations. On the other hand, the usage of engineered skeletal muscle tissues as performed in this work provides design flexibility in biohybrid robots owing to dimension controllability of the skeletal muscle tissues and a longer lifetime of the robot actuations because of the sustainability of the tissues in culture medium. Therefore, engineered skeletal muscle tissues have higher applicability to biohybrid robots than do explanted whole skeletal muscles.

Alternatively, instead of the antagonistic muscle, a mechanical element having stretch characteristics similar to the antagonistic muscle can conceivably be used as an antagonistic structure in the biohybrid robot. However, to achieve long-term actuation under this configuration, the tension of the mechanical element should be adjusted according to the increased tension of the skeletal muscle tissue during culture. By contrast, our biohybrid robot does not require adjustment of the tension because the tensions of both skeletal muscle tissues change in the same way, indicating that the antagonistic pair of skeletal muscle tissues has a suitable configuration for the long-term actuation of the biohybrid robot.

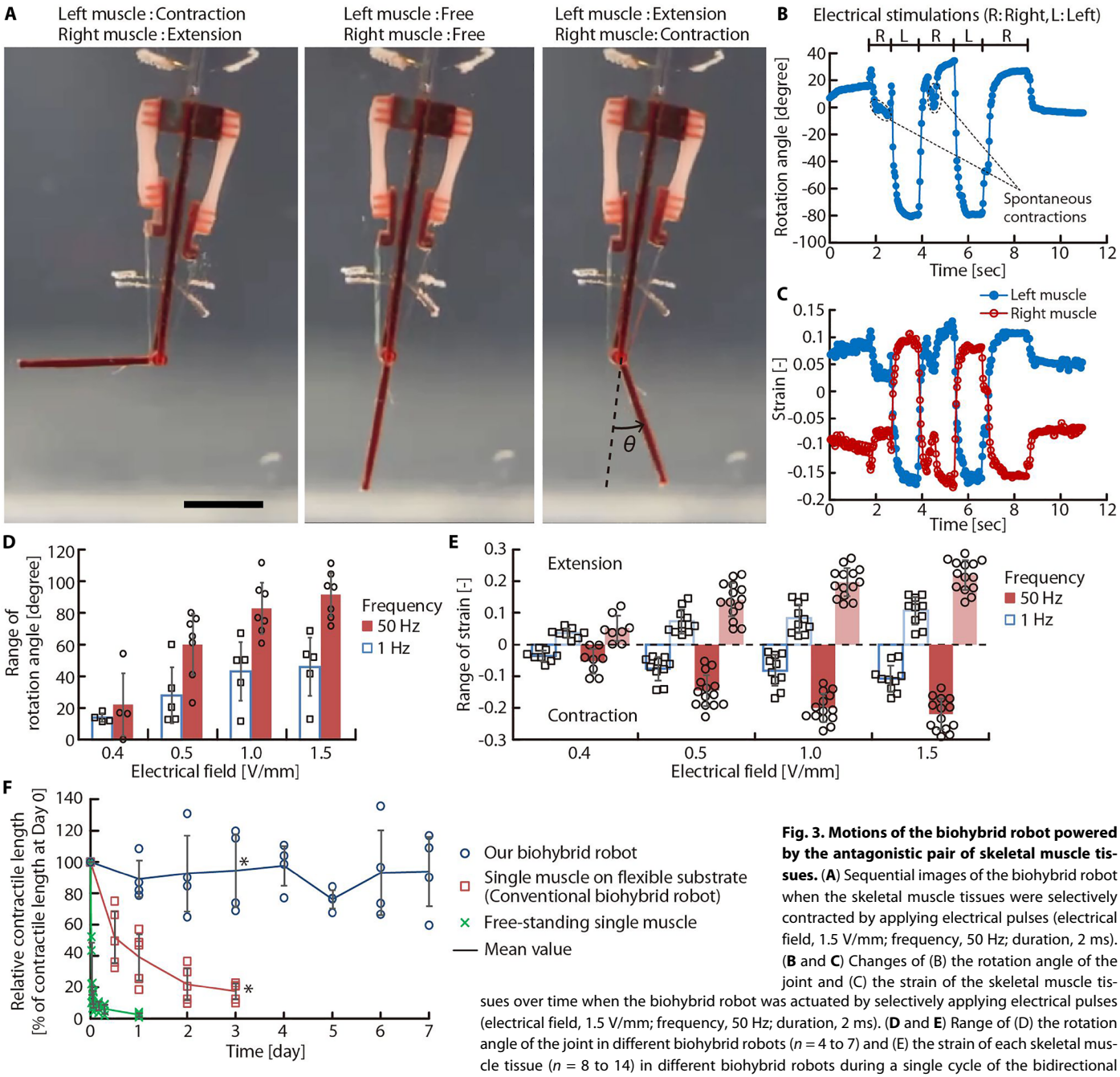


**Fig. 3. Motions of the biohybrid robot powered by the antagonistic pair of skeletal muscle tissues.** (**A**) Sequential images of the biohybrid robot when the skeletal muscle tissues were selectively contracted by applying electrical pulses (electrical field, 1.5 V/mm; frequency, 50 Hz; duration, 2 ms). (**B** and **C**) Changes of (B) the rotation angle of the joint and (C) the strain of the skeletal muscle tissues over time when the biohybrid robot was actuated by selectively applying electrical pulses (electrical field, 1.5 V/mm; frequency, 50 Hz; duration, 2 ms). (**D** and **E**) Range of (D) the rotation angle of the joint in different biohybrid robots ($n$ = 4 to 7) and (E) the strain of each skeletal muscle tissue ($n$ = 8 to 14) in different biohybrid robots during a single cycle of the bidirectional motion achieved by applying electrical pulses (duration, 2 ms). (**F**) Variation with time of the contractile length of one skeletal muscle tissue in different biohybrid robots ($n$ = 4), that of skeletal muscle tissues on flexible substrates ($n$ = 5), and that of free-standing skeletal muscle tissues ($n$ = 4). Electrical pulses (electrical field, 1 V/mm; frequency, 1 Hz; duration, 2 ms) were applied to each tissue. Contractile lengths were normalized according to the contractile length at day 0 of each sample. *$P$ < 0.01, unpaired $t$ test. All error bars show SD. Scale bar, 5 mm.

There is still room for improvement of the actuation and the lifetime of our biohybrid robot. Issues with the actuation of the current design include that the efficiency of converting the contractions of the skeletal muscle tissues into the motions of the biohybrid robot would not be sufficient. Our experimental results show that the configuration of artificial parts in a robot influences its motions. The frictional force of the joint imparts resistance to the contractile movements of skeletal muscle tissues, and errors when manually assembling the skeleton cause length differences in the pair of skeletal muscle tissues. As next steps to achieve smooth and predictable motions in the biohybrid robot, it will be necessary to add biocompatible lubricants to the joint and to establish automated assembly techniques for the biohybrid robot. In addition, issues that could be seen in the lifetime of the biohybrid robot include that electrical stimulations were not optimal to induce the contractions of the skeletal muscle tissues. Bubbles

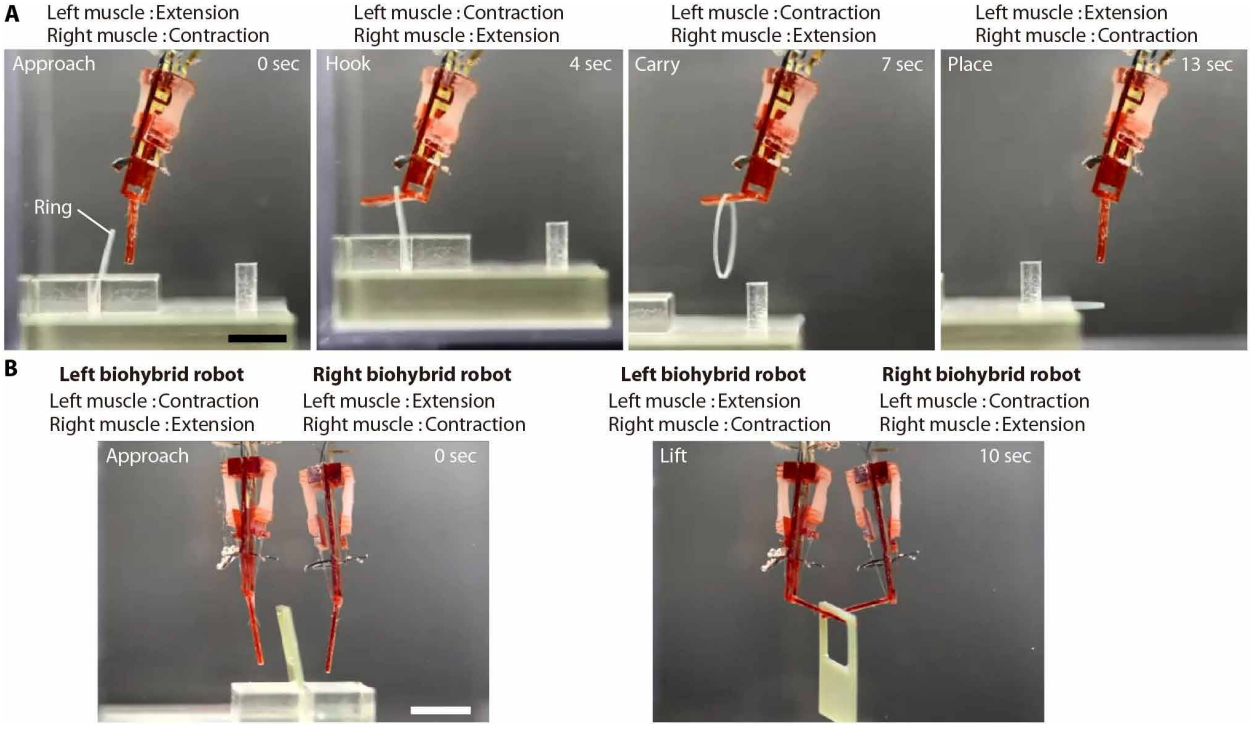


**Fig. 4. Object manipulations performed by our biohybrid robots.** (**A**) Sequential images of a pick-and-place operation of the biohybrid robot by selective contractions of the skeletal muscle tissues generated with electrical pulses (electrical field, 1.5 V/mm; frequency, 50 Hz; duration, 2 ms). (**B**) Sequential images of picking up a square frame by the operation of two biohybrid robots. Skeletal muscle tissues were contracted selectively by applying electrical pulses (electrical field, 1.5 V/mm; frequency, 50 Hz; duration, 2 ms). Scale bars, 1 cm.

generated by electrolysis at the time of the electrical stimulations caused degradation of the skeletal muscle tissues and electrodes. This disadvantage of electrical stimulations limits the long-term and continuous actuation of the biohybrid robot. To overcome these limitations, we consider that it would be effective to use genetically modified skeletal muscle tissues contractible by optical stimulations (*10*, *30*) and skeletal muscle tissues cocultured with motor neurons contractible by neural stimulations (*17*, *31*), because these advanced skeletal muscle tissues can contract via a mechanism similar to that in the skeletal muscles of a living body. In addition, the passive force of skeletal muscle tissues reaches a plateau over 1 week after coculturing with motor neurons (*31*), indicating that spontaneous shrinkage may be easy to prevent in these tissues. For these reasons, integration of the biohybrid robot with these advanced skeletal muscle tissues will increase its lifetime.

For the biofabrication of skeletal muscle tissues, we proposed an original method to construct one skeletal muscle tissue by integration of several myoblast-laden hydrogel sheets after stacking them. The myoblast-laden hydrogel sheets are easier to handle than skeletal muscle tissues because myotube formation is not advanced in the sheets and their spontaneous shrinkage is small. Consequently, our method enables the formation of skeletal muscle tissues at designed positions by manipulation of the sheets. Although we constructed only two skeletal muscle tissues in symmetrical positions on our biohybrid robot, the method allows construction of many skeletal muscle tissues at arbitrary positions to mimic the configuration of living bodies. Therefore, we believe that a biohybrid robot with a more complex composition will be constructable in the future.

This research shows the advantages of a biohybrid robot with an antagonistic pair of skeletal muscle tissues, and the usefulness of this basic concept has been demonstrated. We believe that the results of this work will provide useful knowledge to develop advanced biohybrid robots for biological study of an antagonistic pair of skeletal muscles. Moreover, the concept of this research is applicable to the development of a muscle-on-a-chip system, which is one example of organ-on-a-chip systems composed of culture tissues and perfusable channels, as a model in drug development and toxin testing (*32*). Integration of our biohybrid robot with the muscle-on-a-chip system will enable the development of more physiologically relevant models based on antagonistic pairs of skeletal muscle tissues.

## MATERIALS AND METHODS

### Cell preparation

Single-cell suspensions of myoblasts were prepared from the hindlimbs of Wistar neonatal (1 to 2 days old) rats (Sankyo Labo Service Corporation Inc.) by mechanical trituration using type II collagenase (Invitrogen). All rats were maintained in accordance with the policies of the University of Tokyo Institutional Animal Care and Use Committee.

The growth medium for the myoblasts was composed of Dulbecco's modified Eagle's medium (DMEM; Sigma-Aldrich Co.

LLC) with 10% (v/v) fetal bovine serum (Japan Bioserum Co. Ltd.) and 1% penicillin-streptomycin (Invitrogen). The differentiation medium for the myoblasts was composed of DMEM with 2% (v/v) horse serum (Sigma-Aldrich Co. LLC) and 1% penicillin-streptomycin (Invitrogen).

### Fabrication of skeleton of the biohybrid robot

The skeleton of the biohybrid robot was composed of a substrate with a joint, parylene-coated gold electrodes, anchors for skeletal muscle tissues, and flexible ribbons bridged between the anchors and the joint (fig. S1A). The body of the skeleton with a joint was an assembly of resin parts. The resin parts were fabricated using a commercial stereolithography modeling machine (Perfactory, EnvisionTEC) from a photoreactive acrylate resin (R11, EnvisionTEC). After we exposed the resin parts to ultraviolet (UV) light for over 60 s using a laser machine (UV-LED, Keyence Corp.) for complete curing, we coated them with 2 μm of parylene using a chemical vapor deposition machine (Parylene Deposition System 2010, Specialty Coating Systems Inc.). Afterward, we assembled the resin parts using photoreactive medical adhesive (Loctite 3301, Henkel AG & Co. KGaA) (fig. S1B, i). The parylene-coated gold electrodes were fabricated by patterning gold lines on 10-μm-thick parylene sheets using standard photolithography and were connected with conductive wires using conductive resin (Dotite D-723S, Fujikura Kasei Co. Ltd.). After coating 2 μm of parylene onto the parylene-coated gold electrodes connected with conductive wires to insulate the electrodes other than the tips, we bonded the parylene-coated gold electrodes to the body with a joint using a photoreactive medical adhesive (fig. S1B, ii). Subsequently, we bonded anchors formed by the stereolithography machine to the electrodes using photoreactive medical adhesive (fig. S1B, iii). After mounting PDMS supports to immobilize the anchors, the anchors were connected to flexible ribbons (2-μm-thick parylene ribbons), of which the edges were fixed to the joint using a photoreactive medical adhesive (fig. S1B, iv and v). Last, we coated the anchors with fibronectin (stabilized bovine fibronectin, Thermo Fisher Scientific Inc.) to allow cell adhesion.

### Formation of myoblast-laden hydrogel sheets

For formation of the myoblast-laden hydrogel sheets, we prepared PDMS stamps with grooves. The PDMS stamps were shaped with resin molds. The resin molds were produced by the same method as the resin parts for the skeletons using the stereolithography machine. After UV light exposure and 2 μm of parylene coating, we poured PDMS elastomer (Sylgard 184 Silicone Elastomer, Dow Corning Toray Co. Ltd.) mixed in the ratio of 10:1 (base/cross-linker) into the resin molds. After solidification of the PDMS by heating at 75°C for 90 min, we released the PDMS stamps from the molds. For sterilization of the PDMS stamps, we washed them with ethanol and exposed them to UV light for more than 30 min using a sterilizer machine (sterilizer FV-209B, As One Corporation). Last, the PDMS stamps were treated with ethanol including 0.5 weight % phosphorylcholine-based (MPC) polymers (NOF Corporation) and incubated at 65°C for 90 min to block cell adhesion on the surface of the PDMS stamps.

We used Matrigel as the material for the myoblast-laden hydrogel sheets because myoblasts maintain their differentiation capacity in Matrigel (*33*). After sandwiching 15 μl of Matrigel solution (Corning Incorporated) with myoblasts ($1 \times 10^8$ cells/ml) between the PDMS stamp and a silicone rubber sheet (As One Corporation), we incubated the assembly at 37°C for 15 min to induce gelation of the Matrigel. By releasing the PDMS stamp after 2 days of culture in growth medium, we obtained myoblast-laden hydrogel sheets with striped structures because the myoblasts gradually aggregated in the Matrigel to make sheet structures (fig. S2, A and B).

### Fabrication of biohybrid robots with an antagonistic pair of skeletal muscle tissues

For formation of an antagonistic pair of skeletal muscle tissues on the skeleton with a joint, we mounted the myoblast-laden hydrogel sheets between the anchors by aligning the pillars on the anchors with the holes of the sheets (fig. S1B, vi). In the mounting process, we delivered the silicon rubber sheet with the myoblast-laden hydrogel sheet onto the anchors of the skeleton. After removing the myoblast-laden hydrogel sheet from the silicone rubber sheet, we pushed the myoblast-laden sheet so that the pillars of the anchors passed through the holes at their ends. Repeating this procedure three times, we stacked three myoblast-laden hydrogel sheets on the anchors. The anchors helped the myoblast-laden hydrogel sheets maintain their length against tension. In this state, we used sheets with different striped structures alternately to avoid overlaps of the striped structures (fig. S2C). After culturing the assembly of myoblast-laden hydrogel sheets in growth medium for 1 day, we replaced half of the medium with differentiation medium every day. Last, skeletal muscle tissues were formed on both sides of the biohybrid robot by inducing fusion of the myoblasts into myotubes (fig. S1B, vii). The biohybrid robot was available after removing the PDMS supports to free the anchors (fig. S1B, viii). For OCT imaging of the skeletal muscle tissues, we used an OCT machine (IVS-2000, Santec Corporation).

### Immunostaining

For characterization of the skeletal muscle tissues by immunostaining, after a 10-day culture of the assembly of myoblast-laden hydrogel sheets, biohybrid robots were washed with phosphate-buffered saline (PBS), fixed with 4% paraformaldehyde (PFA; Muto Pure Chemicals Co. Ltd.), permeabilized with 0.1% Triton X-100 (Alfa Aesar) for 20 min, and blocked with 2.5% bovine serum albumin (Sigma-Aldrich Co. LLC) overnight. For immunostaining of α-actinin and myosin heavy chains, we incubated the biohybrid robots with 0.1% monoclonal anti–α-actinin antibody (Sigma-Aldrich Co. LLC) and monoclonal anti-myosin heavy chain antibody (10 μg/ml; R&D Systems Inc.), respectively, at 4°C overnight. Subsequently, we incubated the robots with Alexa Fluor–conjugated secondary antibodies (Thermo Fisher Scientific Inc.) at room temperature for 2 hours. For immunostaining of myogenin, we incubated the biohybrid robots with 1% anti-myogenin Alexa Fluor 488 (eBioscience) at 4°C overnight. After immunostaining, we rinsed them with PBS and stained the cell nuclei with 0.1% Hoechst 33342 (Invitrogen) or DAPI (4′,6-diamidino-2-phenylindole) (Invitrogen). When we observed the immunostained skeletal muscle tissues, we used a laser microscope (LSM 780, Carl Zeiss) for confocal images.

### Sectional images of skeletal muscle tissues

For H&E staining of the skeletal muscle tissues, we first fixed our biohybrid robots with 4% PFA after 10 days culture of the assembly of myoblast-laden hydrogel sheets. Afterward, we removed the skeletal muscle tissues from the biohybrid robots and dipped the

tissues in 30% sucrose solution at 4°C. Then, we froze the tissues in optimal cutting temperature compound (Sakura Finetek Japan Co. Ltd.) and cut them with a cryostat chamber (Hyrax C25, Carl Zeiss) to prepare 8-μm-thick frozen sections. We mounted them on glass slides and stained the sections with Mayer's hematoxylin solution (Wako Pure Chemical Industries Ltd.) and 0.5% eosin Y ethanol solution (Wako Pure Chemical Industries Ltd.). We observed the H&E-stained sections with a microscope (IX71N, Olympus).

### Evaluation of the contractility of skeletal muscle tissues

We estimated the contractile force of the skeletal muscle tissues with PDMS cantilevers using a modified method described previously (*17*, *25*). Briefly, we first placed the skeletal muscle tissue between PDMS cantilevers and fixed the tissue ends on the cantilever tips. We generated an alternative-current square wave as electrical pulses using a function generator (Agilent Technologies Inc.) and an amplifier (Mess-Tek Co. Ltd.) and applied the electrical pulses to gold electrodes placed around the skeletal muscle tissue. As the PDMS cantilever was deformed when the mounted skeletal muscle tissue contracted, we measured the deflection of the cantilever with the microscope and a motion analyzer (VM-9000, Keyence Corp.). We estimated the contractile forces from the deflection of the cantilever because their contractile forces approximate the reaction forces measured from the cantilever according to beam deflection formulas. When we estimated the contractile force in different lengths of skeletal muscle tissues, we changed the length by moving the cantilevers using an *x*-axis stage.

### Motion analysis of the biohybrid robots

Our biohybrid robots were placed in transparent acrylate boxes with phenol red–free DMEM (Sigma-Aldrich Co. LLC) with 1% penicillin-streptomycin for clear observation. To drive the biohybrid robots, we selectively applied electrical pulses to the parylene-coated gold electrodes on both sides of the robot to stimulate the skeletal muscle tissues. The motions of the biohybrid robots were recorded as videos using a digital camera with a macro lens (EOS Kiss X6i, Canon). From the videos, we measured the rotation angle of the joint and the contractile length of each skeletal muscle tissue using the motion analyzer.

### Evaluation of the lifetime of the biohybrid robot motions

To evaluate the lifetime of the biohybrid robots, we placed the robots in transparent acrylate boxes after 5 days of culture with differentiation medium. We applied electrical pulses to the flexor muscle (we defined the shorter skeletal muscle tissues as flexor muscle tissues when the absolute value of the rotation angle was maximized) in the biohybrid robot and recorded the motions of the robot with the same conditions used in the previously described motion analysis. After the experiment, we replaced half of the medium with differentiation medium every day.

For comparison of robots without an antagonistic skeletal muscle tissue, we prepared biohybrid robots with a flexible substrate and free-standing single skeletal muscle tissues. To prepare the biohybrid robot with a flexible substrate, we fixed the anchors onto the parylene-coated gold electrodes using photoreactive medical adhesive. We immobilized the parylene-coated gold electrodes onto the surface of culture dishes and formed a skeletal muscle tissue on the anchors by culturing three stacked myoblast-laden hydrogel sheets for 5 days (fig. S9B). After releasing the parylene-coated gold electrodes from the culture dishes, we observed their motion using the same method described for observation of our biohybrid robot, and we replaced half of the medium with differentiation medium every day. To form the free-standing single skeletal muscle tissue, we cultured three stacked myoblast-laden hydrogel sheets for 5 days on the anchors immobilized with a PDMS substrate (fig. S9C). After releasing the skeletal muscle tissues from the PDMS substrate, we applied electrical pulses to the tissues in culture dishes and recorded their contractions as videos using the microscope.

In the experiments, we used the motion analyzer to quantify the contractile length of the skeletal muscle tissues in every sample, the rotation angle of our biohybrid robots, and the angle of the biohybrid robot with a flexible substrate, as shown in fig. S9H. Unpaired *t* test was used to compare the relative contractile lengths (percentage of contractile length at day 0) of skeletal muscle tissues in the biohybrid robots with that of skeletal muscle tissues on flexible substrates at day 3.

### Manipulation of objects using biohybrid robots

For demonstration of object manipulation using our biohybrid robots, we fabricated a ring, a square frame, and substrates for immobilization of the ring and the square frame using a 3D printer (AGILISTA-3200, Keyence Corp.). We placed the ring on the substrate in the demonstration using a single biohybrid robot and placed the square frame on the substrate in the demonstration of an operation of two biohybrid robots. The biohybrid robots were driven by applying electrical pulses with the same conditions used in the motion analyses of the biohybrid robots in the transparent acrylate box. For lifting and carrying the objects, locomotion of the biohybrid robots was performed by moving the box with a *z*-axis stage and an *x*-axis stage.

## SUPPLEMENTARY MATERIALS

robotics.sciencemag.org/cgi/content/full/3/18/eaat4440/DC1

Section S1. Relationship between the motions of our biohybrid robot and the contractile properties of the skeletal muscle tissues

Fig. S1. Fabrication process of our biohybrid robot.

Fig. S2. Detailed process for stacking the myoblast-laden hydrogel sheets.

Fig. S3. Formation of skeletal muscle tissue on our biohybrid robot.

Fig. S4. Observation of our biohybrid robot.

Fig. S5. Contractile properties of the striped patterned skeletal muscle tissues.

Fig. S6. Confocal image of a skeletal muscle tissue immunostained with α-actinin, myogenin, and the cell nucleus.

Fig. S7. Schematic illustration for comparison of a myoblast-laden hydrogel block and a stack of myoblast-laden hydrogel sheets.

Fig. S8. Selective contractions of the skeletal muscle tissue in the biohybrid robot.

Fig. S9. Variation with time of the motions of our biohybrid robot, a conventional biohybrid robot, and a free-standing single skeletal muscle tissue.

Fig. S10. Calculated balance between the flexor muscle and extensor muscle.

Movie S1. Bidirectional motions of our biohybrid robot.

Movie S2. Motions of our biohybrid robot under applied electrical pulses (50 Hz, 2 ms) with different magnitudes of the electrical field.

Movie S3. Pick-and-place operation by a single biohybrid robot.

Movie S4. Pick-up operation achieved by two biohybrid robots.

## REFERENCES AND NOTES

1. A. W. Feinberg, Biological soft robotics. *Annu. Rev. Biomed. Eng.* **17**, 243–265 (2015).
2. J. U. Lind, T. A. Busbee, A. D. Valentine, F. S. Pasqualini, H. Yuan, M. Yadid, S.-J. Park, A. Kotikian, A. P. Nesmith, P. H. Campbell, J. J. Vlassak, J. A. Lewis, K. K. Parker, Instrumented cardiac microphysiological devices via multimaterial three-dimensional printing. *Nat. Mater.* **16**, 303–308 (2017).

3. Y. Sun, R. Duffy, A. Lee, A. W. Feinberg, Optimizing the structure and contractility of engineered skeletal muscle thin films. *Acta Biomater.* **9**, 7885–7894 (2013).
4. Y. Tanaka, K. Sato, T. Shimizu, M. Yamato, T. Okano, T. Kitamori, A micro-spherical heart pump powered by cultured cardiomyocytes. *Lab Chip* **7**, 207–212 (2007).
5. K.-i. Kabumoto, T. Hoshino, Y. Akiyama, K. Morishima, Voluntary movement controlled by the surface EMG signal for tissue-engineered skeletal muscle on a gripping tool. *Tissue Eng. Part A* **19**, 1695–1703 (2013).
6. T. Hoshino, K. Morishima, Muscle-powered cantilever for microtweezers with an artificial micro skeleton and rat primary myotubes. *J. Biomech. Sci. Eng.* **5**, 245–251 (2010).
7. A. W. Feinberg, A. Feigel, S. S. Shevkoplyas, S. Sheehy, G. M. Whitesides, K. K. Parker, Muscular thin films for building actuators and powering devices. *Science* **317**, 1366–1370 (2007).
8. V. Chan, K. Park, M. B. Collens, H. Kong, T. A. Saif, R. Bashir, Development of miniaturized walking biological machines. *Sci. Rep.* **2**, 857 (2012).
9. C. Cvetkovic, R. Raman, V. Chan, B. J. Williams, M. Tolish, P. Bajaj, M. S. Sakar, H. H. Asada, M. T. A. Saif, R. Bashir, Three-dimensionally printed biological machines powered by skeletal muscle. *Proc. Natl. Acad. Sci. U.S.A.* **111**, 10125–10130 (2014).
10. R. Raman, C. Cvetkovic, S. G. M. Uzel, R. J. Platt, P. Sengupta, R. D. Kamm, R. Bashir, Optogenetic skeletal muscle-powered adaptive biological machines. *Proc. Natl. Acad. Sci. U.S.A.* **113**, 3497–3502 (2016).
11. J. C. Nawroth, H. Lee, A. W. Feinberg, C. M. Ripplinger, M. L. McCain, A. Grosberg, J. O. Dabiri, K. K. Parker, A tissue-engineered jellyfish with biomimetic propulsion. *Nat. Biotechnol.* **30**, 792–797 (2012).
12. B. J. Williams, S. V. Anand, J. Rajagopalan, M. T. A. Saif, A self-propelled biohybrid swimmer at low Reynolds number. *Nat. Commun.* **5**, 3081 (2014).
13. S.-J. Park, M. Gazzola, K. S. Park, S. Park, V. Di Santo, E. L. Blevins, J. U. Lind, P. H. Campbell, S. Dauth, A. K. Capulli, F. S. Pasqualini, S. Ahn, A. Cho, H. Yuan, B. M. Maoz, R. Vijaykumar, J.-W. Choi, K. Deisseroth, G. V. Lauder, L. Mahadevan, K. K. Parker, Phototactic guidance of a tissue-engineered soft-robotic ray. *Science* **353**, 158–162 (2016).
14. M. T. Holley, N. Nagarajan, C. Danielson, P. Zorlutuna, K. Park, Development and characterization of muscle-based actuators for self-stabilizing swimming biorobots. *Lab Chip* **16**, 3473–3484 (2016).
15. H. Vandenburgh, J. Shansky, F. Benesch-Lee, V. Barbata, J. Reid, L. Thorrez, R. Valentini, G. Crawford, Drug-screening platform based on the contractility of tissue-engineered muscle. *Muscle Nerve* **37**, 438–447 (2008).
16. L. Rao, Y. Qian, A. Khodabukus, T. Ribar, N. Bursac, Engineering human pluripotent stem cells into a functional skeletal muscle tissue. *Nat. Commun.* **9**, 126 (2018).
17. Y. Morimoto, M. Kato-Negishi, H. Onoe, S. Takeuchi, Three-dimensional neuron–muscle constructs with neuromuscular junctions. *Biomaterials* **34**, 9413–9419 (2013).
18. W. Bian, N. Bursac, Engineered skeletal muscle tissue networks with controllable architecture. *Biomaterials* **30**, 1401–1412 (2009).
19. S. Hinds, W. Bian, R. G. Dennis, N. Bursac, The role of extracellular matrix composition in structure and function of bioengineered skeletal muscle. *Biomaterials* **32**, 3575–3583 (2011).
20. S. Zatti, A. Zoso, E. Serena, C. Luni, E. Cimetta, N. Elvassore, Micropatterning topology on soft substrates affects myoblast proliferation and differentiation. *Langmuir* **28**, 2718–2726 (2012).
21. M. Juhas, G. C. Engelmayr Jr., A. N. Fontanella, G. M. Palmer, N. Bursac, Biomimetic engineered muscle with capacity for vascular integration and functional maturation in vivo. *Proc. Natl. Acad. Sci. U.S.A.* **111**, 5508–5513 (2014).
22. R. G. Dennis, P. E. Kosnik II, Excitability and isometric contractile properties of mammalian skeletal muscle constructs engineered in vitro. *In Vitro Cell. Dev. Biol. Anim.* **36**, 327–335 (2000).
23. Y. Yamamoto, A. Ito, H. Fujita, E. Nagamori, Y. Kawabe, M. Kamihira, Functional evaluation of artificial skeletal muscle tissue constructs fabricated by a magnetic force-based tissue engineering technique. *Tissue Eng. Part A* **17**, 107–114 (2011).
24. L. Ricotti, B. Trimmer, A. W. Feinberg, R. Raman, K. K. Parker, R. Bashir, M. Sitti, S. Martel, P. Dario, A. Menciassi, Biohybrid actuators for robotics: A review of devices actuated by living cells. *Sci. Robot.* **2**, eaaq0495 (2017).
25. Y. Morimoto, S. Mori, F. Sakai, S. Takeuchi, Human induced pluripotent stem cell-derived fiber-shaped cardiac tissue on a chip. *Lab Chip* **16**, 2295–2301 (2016).
26. A. F. Huxley, Muscular contraction. *J. Physiol.* **243**, 1–43 (1974).
27. D. Sangian, S. Naficy, G. M. Spinks, B. Tondu, The effect of geometry and material properties on the performance of a small hydraulic McKibben muscle system. *Sens. Actuators A Phys.* **234**, 150–157 (2015).
28. W. Lowe, *Orthopedic Assessment in Massage Therapy* (David Scott, 2006).
29. H. Herr, R. G. Dennis, A swimming robot actuated by living muscle tissue. *J. Neuroeng. Rehabil.* **1**, 6 (2004).
30. M. S. Sakar, D. Neal, T. Boudou, M. A. Borochin, Y. Li, R. Weiss, R. D. Kamm, C. S. Chen, H. H. Asada, Formation and optogenetic control of engineered 3D skeletal muscle bioactuators. *Lab Chip* **12**, 4976–4985 (2012).
31. S. G. M. Uzel, R. J. Platt, V. Subramanian, T. M. Pearl, C. J. Rowlands, V. Chan, L. A. Boyer, P. T. C. So, R. D. Kamm, Microfluidic device for the formation of optically excitable, three-dimensional, compartmentalized motor units. *Sci. Adv.* **2**, e1501429 (2016).
32. G. Agrawal, A. Aung, S. Varghese, Skeletal muscle-on-a-chip: An in vitro model to evaluate tissue formation and injury. *Lab Chip* **17**, 3447–3461 (2017).
33. S. Grefte, A. Vullinghs, A. M. Kuijpers-Jagtman, R. Torensma, J. W. Von den Hoff, Matrigel, but not collagen I, maintains the differentiation capacity of muscle derived cells in vitro. *Biomed. Mater.* **7**, 055004 (2012).


**Acknowledgments:** We thank M. Onuki, M. Kiyosawa, and F. Takemura for technical support in the preparation of myoblasts and fabrication of devices. The OCT machine (IVS-2000, Santec Corporation) was provided with courtesy from the Santec Corporation. **Funding:** This research was partially supported by the Japan Society for the Promotion of Science Grants-in-Aid for Scientific Research (KAKENHI) (grant nos. JP16H06329 and JP17H04805) and Takeuchi Biohybrid Innovation Project, Exploratory Research for Advanced Technology, Japan Science and Technology Agency (grant no. JPMJER1003). **Author contributions:** All authors planned the experiment and contributed to the analysis of the data and discussion. Y.M. performed and H.O. supervised the experiment. Y.M. and S.T. wrote the paper. **Competing interests:** The authors declare that they have no competing interests. **Data and materials availability:** All data are presented in the paper and/or in the Supplementary Materials. Contact S.T. for additional information.

Submitted 27 February 2018
Accepted 30 April 2018
Published 30 May 2018
10.1126/scirobotics.aat4440

**Citation:** Y. Morimoto, H. Onoe, S. Takeuchi, Biohybrid robot powered by an antagonistic pair of skeletal muscle tissues. *Sci. Robot.* **3**, eaat4440 (2018).

Science Robotics

# Biohybrid robot powered by an antagonistic pair of skeletal muscle tissues

Yuya Morimoto, Hiroaki Onoe, and Shoji Takeuchi

*Sci. Robot.* **3** (18), eaat4440. DOI: 10.1126/scirobotics.aat4440







*Science Robotics* (ISSN 2470-9476) is published by the American Association for the Advancement of Science. 1200 New York Avenue NW, Washington, DC 20005. The title *Science Robotics* is a registered trademark of AAAS.